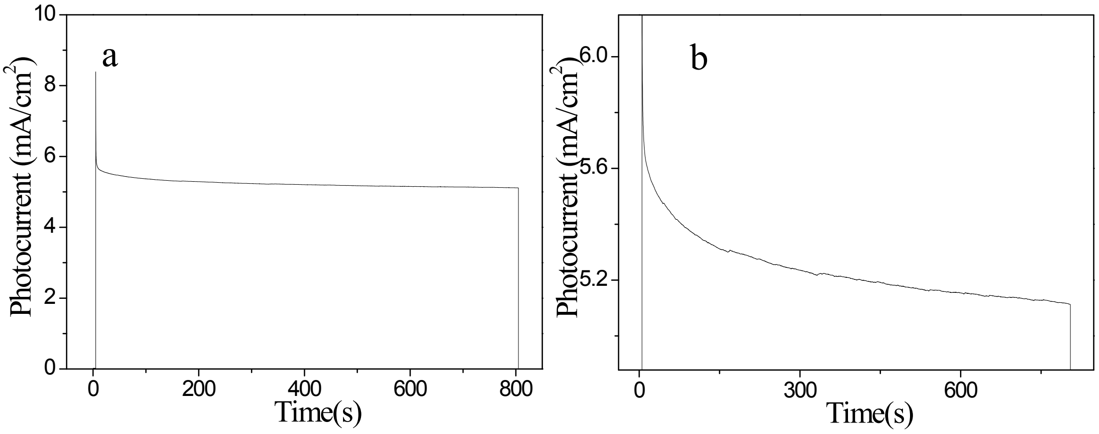

Figure s1. i-t curves of R-TiO$_2$ measured at 0.6V (vs.Ag/AgCl) for 800 seconds, (b) is the enlarged part of (a).

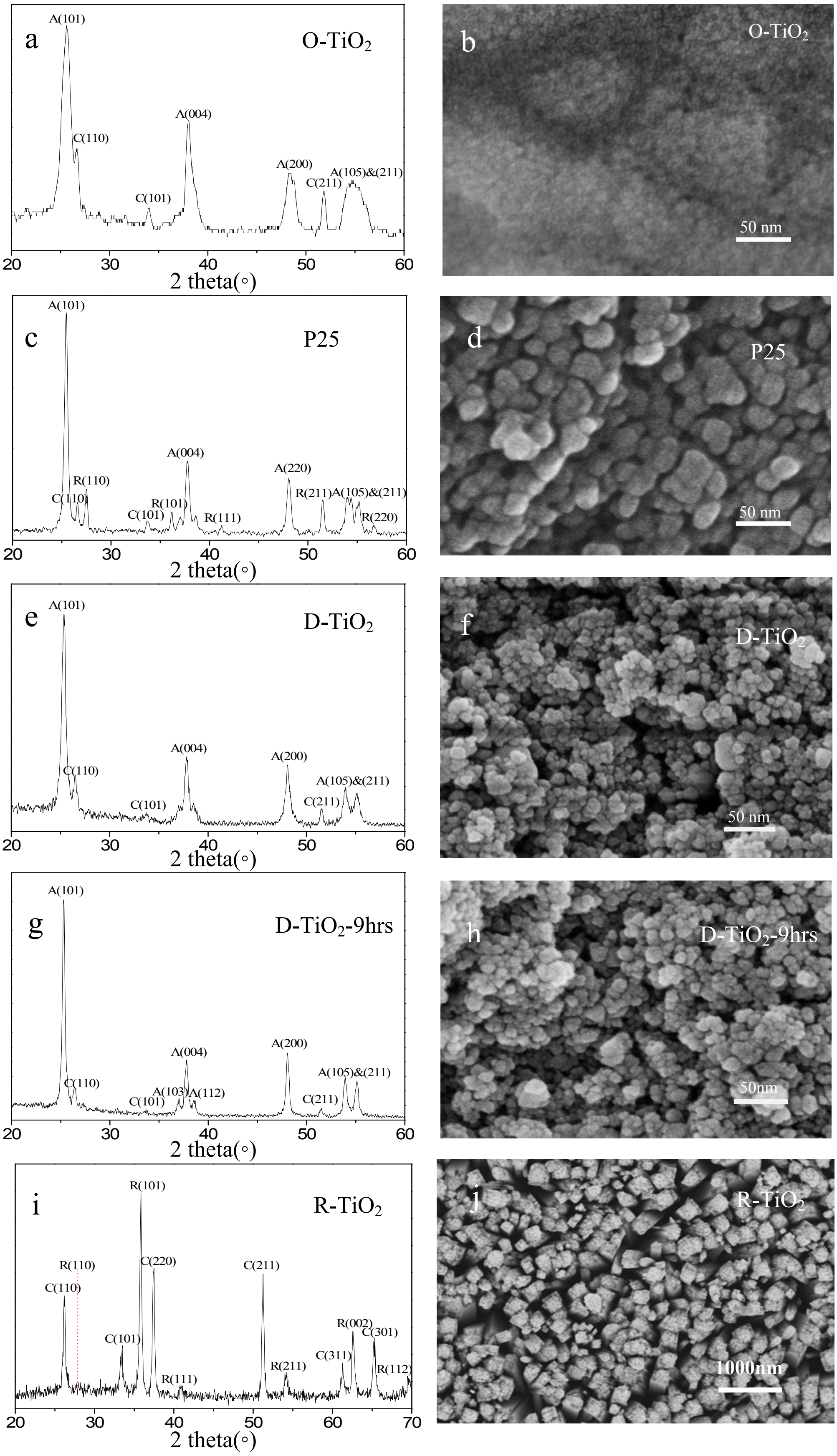

Figure s2. XRD spectra and SEM images of (a) and (b) O-TiO$_2$,[1] (c) and (d) P25, (e) and (f) D-TiO$_2$, (g) and (h) D-TiO$_2$-9hrs, (i) and (j) R-TiO$_2$. Inset are the miller index where “A” refers to *anatase* TiO$_2$, “R” to *rutile* TiO$_2$ and “C” to *cassiterite* SnO$_2$ from FTO.

Table s1. Structural information of the TiO_2 films used in this work.

Film[a]	Phase	Particle Size (nm)	Particle shape	C_{dl} ($mF \cdot cm^{-2}$)	EASA (cm^2)[b]
O-TiO_2	*Anatase*	6.7	spherical	1.39	18.53
P25	*Anatase/Rutile*	20	spherical	1.33	17.73
D-TiO_2	*Anatase*	16.4	spherical	11.4	76.0
D-TiO_2-9hrs	*Anatase*	16.7	spherical	11.2	74.67
R-TiO_2	*Rutile*	250	Rod-like	0.748	4.99

[a] The O-TiO_2 and P25 films are prepared through the doctor-blade method; the O-TiO_2 particles are prepared following the procedure in reference 1.

[b] Assuming the EASA of FTO to be 1 cm^2.

S1: Discussion on the structure of the R-TiO_2 films.

XRD and SEM characterizations prove that the R-TiO_2 film is constructed with *rutile* TiO_2 rods with a diameter of *ca.* 250nm (Fig.s2i and j). Moreover, the usually strongest diffraction R(110) at 27.4° is almost totally disappeared, and the secondary strong diffraction R(211) at 54.3° is greatly weakened. On the contrary, the usually weak diffraction R (002) is enhanced (Fig.s2i). These information indicate that the R-TiO_2 film is composed of an array of rutile TiO_2 single crystal rods with the axial [001] direction perpendicular to FTO surface.[2]

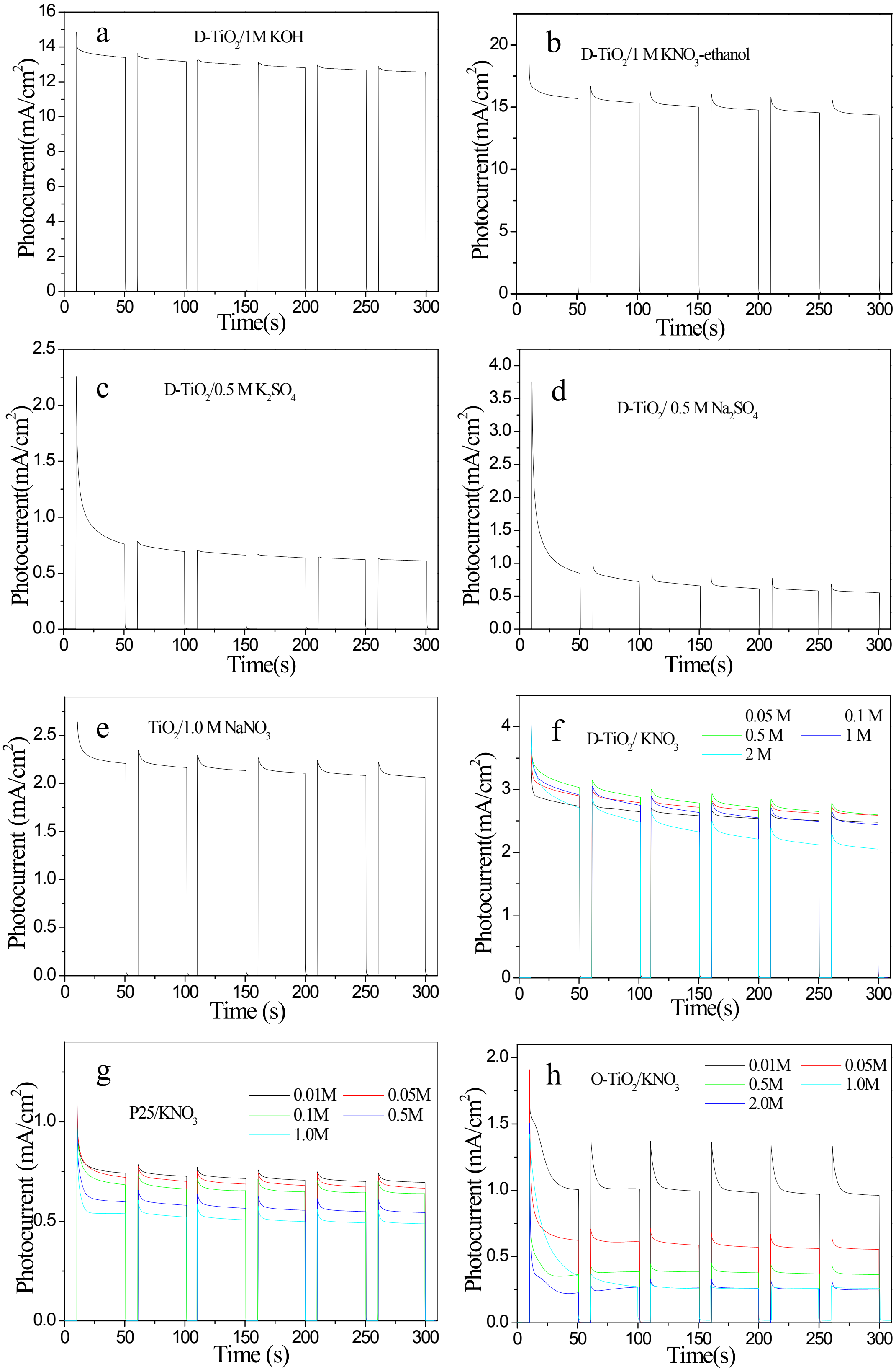

Figure s3. The i-t curves measured using different TiO_2 films or in different electrolytes, (a) D-TiO_2/KOH(1.0M);(b) D-TiO_2/KNO_3 (1.0M, 27ml)-ethanol (3ml); (c) D-TiO_2/K_2SO_4 (0.5M); (d) D-TiO_2/Na_2SO_4 (0.5M); (e)D-TiO_2/$NaNO_3$ (1.0M);(f) D-TiO_2/ KNO_3 (0.05~2.0M); (g) P25/KNO_3 (0.01~1.0M); (h) O-TiO_2/ KNO_3 (0.01~2.0M).

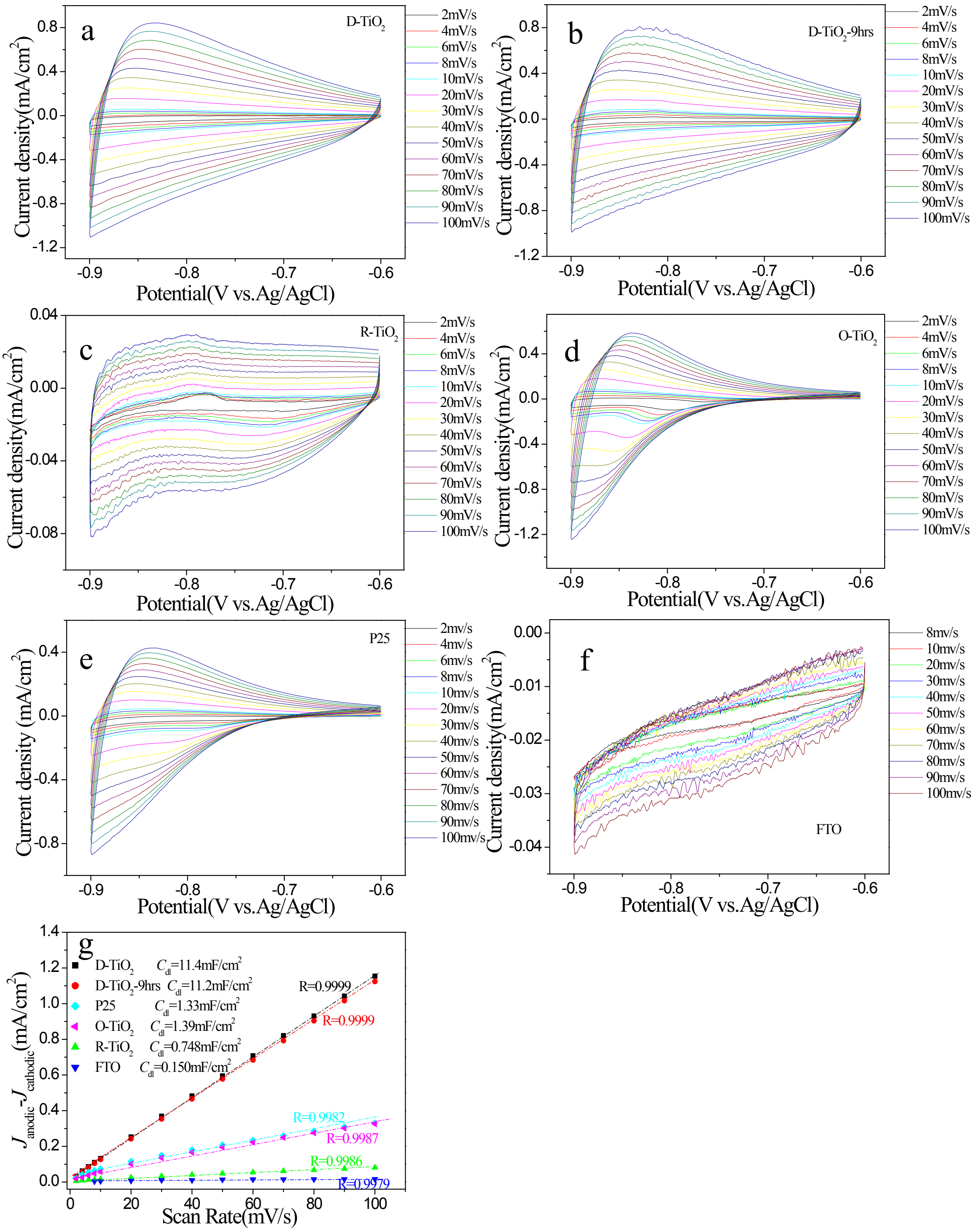

Figure s4. (a)~(f) cyclic voltammograms recorded for the TiO_2 and FTO electrodes in the region of -0.9~-0.6 V vs. Ag/AgCl at various scan rates for the purpose to determine the double layer capacitance (C_{dl}). (g) Dependence of $J_{anodic} - J_{cathodic}$ on CV scan rate to extract C_{dl} for FTO and these TiO_2 films at -0.75 V where TiO_2 films behave like conductors. Note that the fluctuations in the CV curves in Fig.s4c and f are related to both the much smaller current value and N_2 bubbling during the CV measurements.

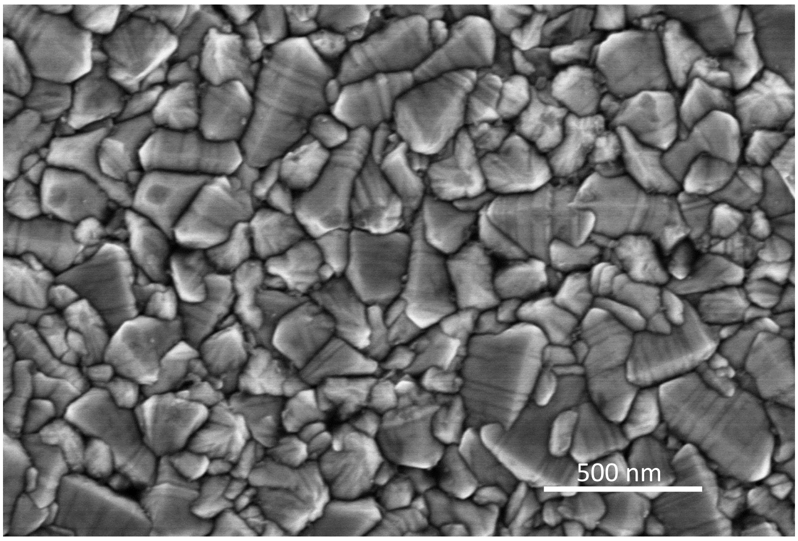

Figure s5. SEM image of the conducting surface of FTO glass.

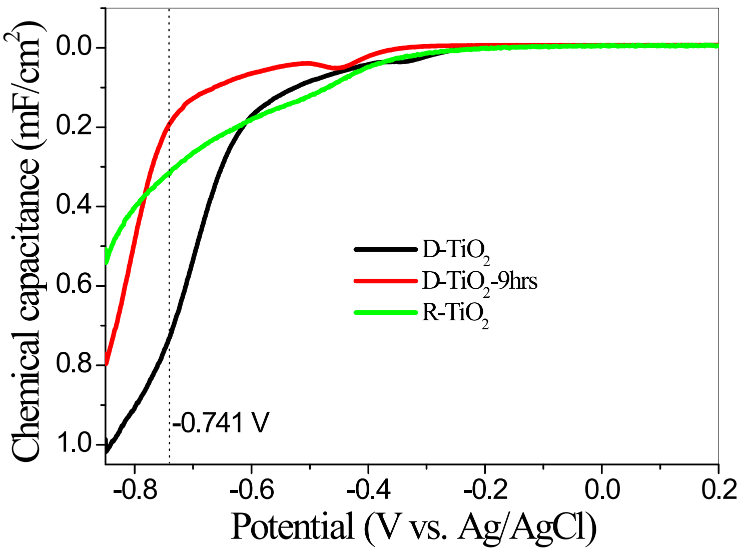

Figure s6. Dependence of the chemical capacitance (C_{μ}) in per unit EASA (1 cm^2) on potential with the purpose of showing the distribution of the density of defect states (DODS) in the band gap of the TiO_2 films. The dot lines marks the conduction band edge at -0.741V.

S2. Excluding two possible reasons of the continuous photocurrent decay

1. Electron acceptors (O_2 and other oxidation products) accumulating in film's pore

Electron acceptors such as O_2 and other oxidation products are formed and maybe accumulated in film's pores during water oxidation process, which can be another reason of the decay. If that is the truth, the decay will depend on pore structure, moreover, a larger photocurrent will lead to more electron acceptors accumulated in pores, and consequently will cause much faster decay of photocurrent.

Both the D-TiO_2 and D-TiO_2-9hrs films have the quite close structure and morphologies (Fig.s2e~h and Tab.s1). The 9-hours heat treatment makes the photocurrents (at 250s) rise from 1.45 (D-TiO_2) to 1.79 mA/cm^2 (D-TiO_2-9hrs) while makes the decay rates (with the photocurrent at 50s as the initial value) reduced from 21.6% for D-TiO_2 to 13.1% for D-TiO_2-9hrs (Fig.s7). The fact that the photocurrent increasing is accompanied with the slowing down of the decay implies that accumulation of electron acceptors in pore is not a decisive factor to the photocurrent decay at least in the current system.

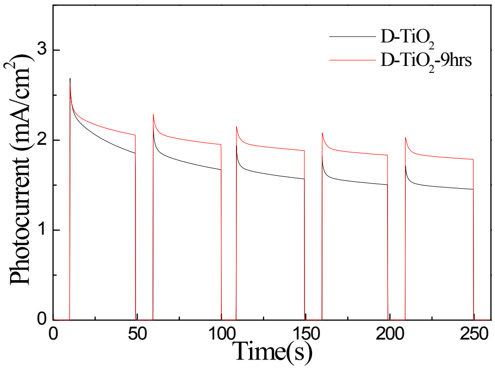

Figure s7. i-t curves of D-TiO_2 and D-TiO_2-9hrs measured in 1M KNO_3 and the bias is 0.6V (vs.Ag/AgCl).

2. Fermi level pinning

For nanostructured semiconductor electrodes, another photoactivity decay mechanism is related to Fermi level pinning.[3] This effect makes the applied bias mainly consumed at the electrolyte side and the energy band bending in semiconductor and photovoltage become smaller.[4] A series of combined i-t/cyclic voltammetry (CV) and i-t/Mott-Schottky (M-S) measurements prove that electrolyte/electrode interface quickly reaches a static quasi-equilibrium status and the energy band edges are fixed (Fig.s8, s9). It has been reported that in metal oxide semiconductors, the surface state DOS is generally small and Fermi level pinning is rarely observed.[5] Therefore, the Fermi level pinning effect is not the reason of the photocurrent decay.

Cyclic voltammetry (CV) or Mott-Schottky (M-S) measurements are carried out in dark immediately after the i-t processes proceeding for a certain periods of time. The combined measurements are controlled automatically with macro command programs, and there is no time interval between them (i-t/CV or i-t/M-S).

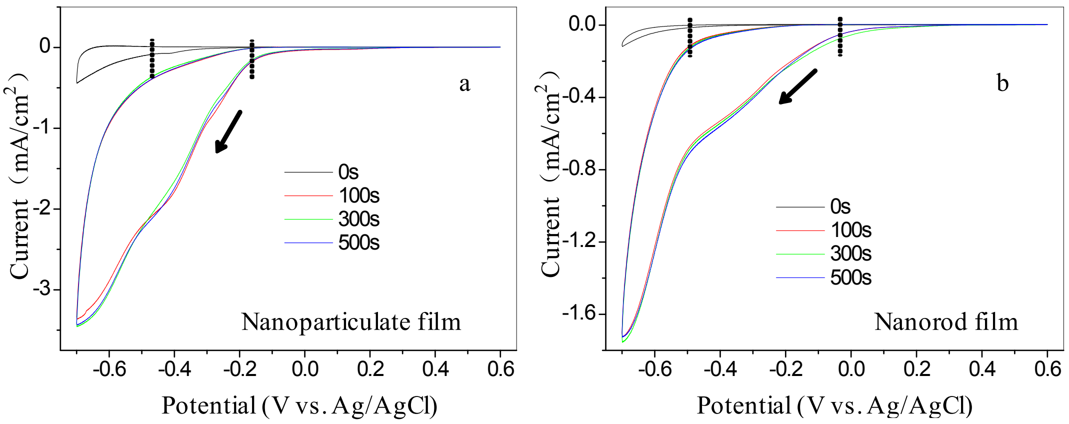

Figure s8. The CV curves of (a) D-TiO_2 and (b) R-TiO_2 electrodes from the combined i-t and CV measurements. Inset are the seconds of each i-t testing. The scanning rate is 0.1V/s. The arrows mark the scanning orientation. The dashed lines mark roughly $E_{fb\text{-}FTO}$.

The negative current in CV increases continuously when the potential bias is scanned negatively. Considering the thermodynamic potential of water reduction reaction ($H_2O + e^- = OH^- + 1/2H_2$) under neutral (pH=7) electrolyte condition is calculated to be -0.61V (vs Ag/AgCl) and the usually high overpotential of hydrogen evolution reaction (HER), the cathodic currents cannot be resulted from HER but from electron filling the intra band gap/conduction band states of TiO_2 and then being extracted by O_2 molecules which are formed during the i-t processes.[6-8]

After the potentials marked with the dashed lines in Fig.s8 the increase of the negative currents get faster. The marked potentials correspond to the flattening of FTO conduction band, under this situation the Schottky barrier is diminished and electrons flow from FTO to TiO_2 with the lowest resistance. The negative currents after the onset potential increases exponentially, which is indicative of the distribution of the density of intra band gap states of TiO_2 (DOS).[6] Fig.s8 shows that the distribution of DOS of TiO_2 is cathodically shift after subjecting to a 100s i-t process. Moreover, prolonging the i-t process can not change them any longer since the CV curves are almost coincident.

Fig.s9 shows the evolutions of the Mott-Schottky (M-S) curves of the two TiO_2-FTO electrodes along with the proceeding of the i-t processes. The M-S measurements are carried out in dark immediately after a certain period of i-t process. The flat band potentials (V_{fb}) are derived from the horizontal-axis intercept of the linear part of the M-S curves. Note that M-S plot for capacitance at 1kHz of D-TiO_2 film corresponds to FTO substrate (not TiO_2 nanoparticles), with $N_d \sim 10^{20}$-10^{21}cm^{-3}.[9] In fact, TiO_2 nanoparticles do not produce a M-S unless highly doped, which is not the case herein. Instead they produce chemical capacitance that changes exponentially with potential.[10] Therefore, the flat band potential derived from the M-S measurements can be assigned to the FTO, $V_{fb\text{-}FTO}$.

Fig.s9 further confirms that the i-t process can shift $V_{fb\text{-}FTO}$ cathodically. Moreover, it is a very slow progress (at least 30 minutes) for the electrode to restore to its initial $V_{fb\text{-}FTO}$ value while each M-S measurement only takes 36 seconds. Therefore, the $V_{fb\text{-}FTO}$ derived from the immediate and fast M-S measurement in dark condition should be very close to the real-time $V_{fb\text{-}FTO}$ at the time point when the PEC process is just finished, if they are not totally the same. Consistent with Fig.s8, Fig.s9 also proves that the $V_{fb\text{-}FTO}$ is fixed along with the proceeding of the i-t processes.

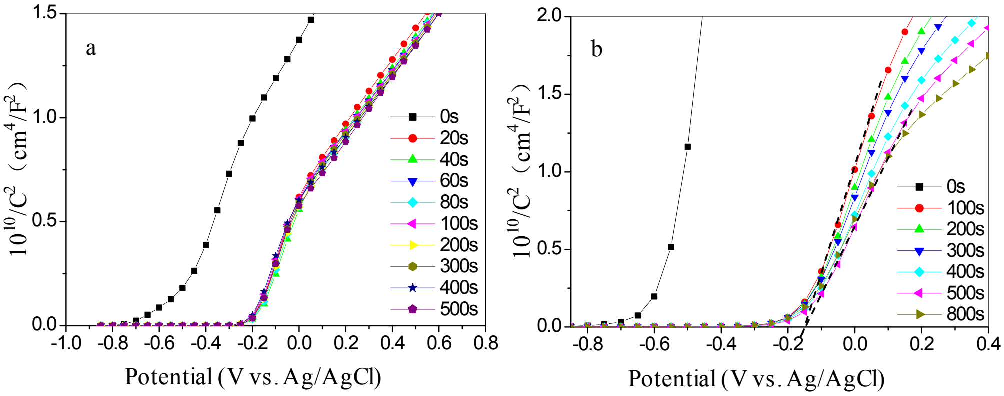

Figure s9. The Mott-Schottky curves of (a) D-TiO_2 and (b) R-TiO_2 electrodes from the combined i-t and M-S measurements. Inset are the time of each i-t testing. The frequency for M-S measurement is 1000 Hz, amplitude is 10 mV. The calculated N_d is *ca.* 4.8×10^{20} cm^{-3} for D-TiO_2, *ca.* 1.2×10^{20} cm^{-3} for R-TiO_2 in dark and $2.2\sim3.2\times10^{20}$ cm^{-3} for R-TiO_2 after i-t processes.

The cathodic shift of the $V_{fb\text{-}FTO}$ is probably resulted from the i-t process induced alteration of the charge distribution at the interface. During the i-t process, a +0.6V bias is applied and water oxidation reactions take place. Thus, O_2 molecules are released and H^+ concentration raises at TiO_2 surface. This local change of pH is the origin of the initial shift of the $V_{fb\text{-}FTO}$ and the distribution of DOS in TiO_2. While, both Fig.s8 and s9 reveal that prolonging the i-t process does not further change them any more, proving that electrolyte/electrode interface quickly reaches a static quasi-equilibrium status and the energy band edges are fixed.

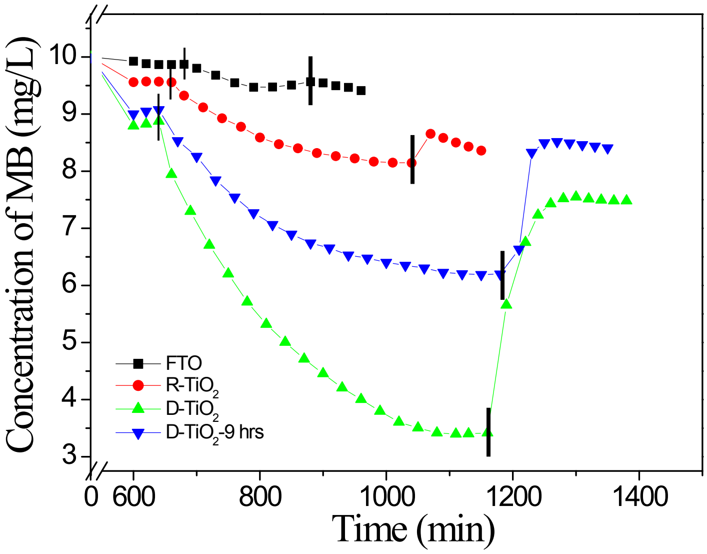

Figure s10. Time dependent evolution of MB's concentration during the electron trapping experiments. In the time range before the thin line, the system is in open circuit status. A -0.8V bias is applied between the thin line and the thick line. After the thick line the bias is shifted to 0.8V.

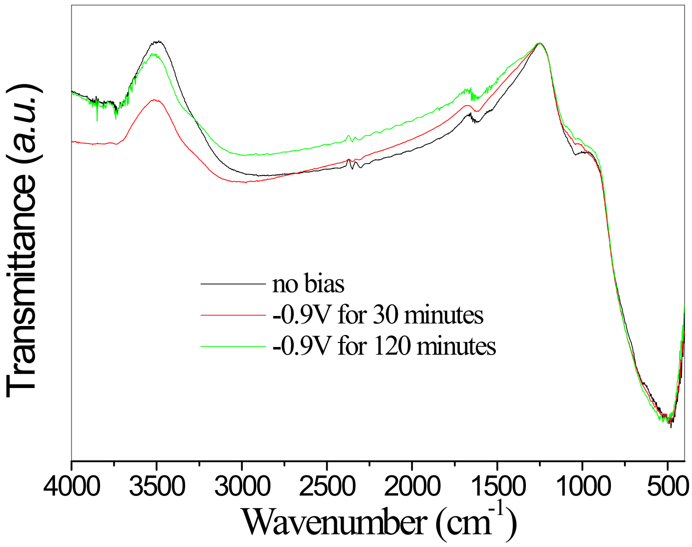

Figure s11. IR spectra of the phosphate-modified TiO_2 after subjecting to electron trapping at -0.9V for different period of time.

S3. Combined measurements of i-t under UV exposure and Potential-step chronoamperometry (PSCA) in dark.

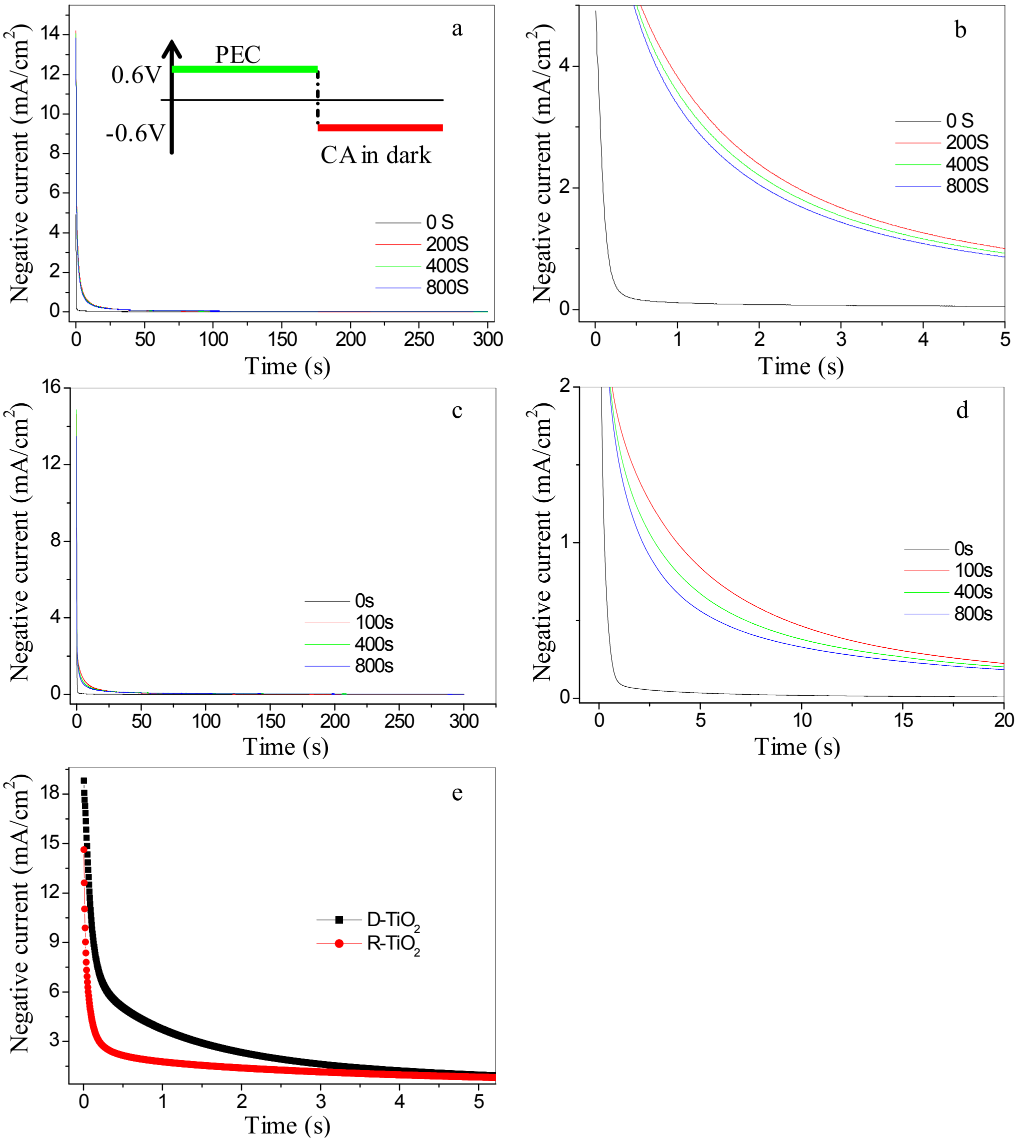

Figure s12. Negative current transient curves from a series of combined i-t and PSCA measurements: (a) D-TiO_2 film, (b) the enlarged part in (a), (c) R-TiO_2 film, (d) the enlarged part in (c). Inset in (a) is the time scheme of the potential step, the duration of the CA in dark is 300s. (e) The CA transient curves of D-TiO_2 and R-TiO_2 films measured immediately after subjecting to a 100s i-t process, the two films have the same amount of TiO_2, *ca.*0.0030g/cm^2.

Fig.s12 shows the current transients of both D-TiO_2 and R-TiO_2 film from a series of the combined i-t/PSCA measurements. After a certain period of i-t process under UV irradiation and at 0.6V bias, an immediate shift of the bias from 0.6V to -0.6V in dark gives a negative current transient. During the i-t processes the $V_{fb\text{-}FTO}$ (as well as the distribution of DOS of TiO_2)) is fixed at -0.20V (Fig.s8 and Fig.s9). Therefore, the negative current transients are resulted from electrons injecting into TiO_2 films when applying -0.6V bias.

The black curve in Fig.s12a~d shows the current transient measured without subjecting to the i-t process before (the time of i-t is 0s). The i-t processes make the current values of the transient curves increase remarkably (colored curves). It can be assigned to the positive shift of the band edge during the i-t processes (Fig.s8 and s9). The integral of the transient curves gives the amount of injected charge (which is the sum of that accumulated in D-TiO_2 and that extracted by electron acceptor such as O_2) after bias is shifted from 0.6 to -0.6V. (Tab.s2). It can be seen from Tab.s2 that the amounts of the injected charge are roughly the same though the duration of the i-t processes is quite different. This indicates the chemical capacitance (and thus the DOS) is not further changed along with the proceeding of the i-t processes, consistent with that of the combined i-t/CV measurements (Fig.s8). Fig.s12e proves that the D-TiO_2 film has much larger amount of trap states than that of the R-TiO_2 film (both have the same mass of TiO_2, ca. 0.0030g/cm^2).

Table s2. The amount of injected charge derived by integrating the transient curves. "Time" refers to the duration of i-t process under UV light irradiation.

Sample	D-TiO_2			R-TiO_2		
Time (s)	200	400	800	100	400	800
Charge (mC)	30.6	31.0	31.3	21.7	22.9	20.8

***Note that*: These current transients can be used to evaluate the evolution of electron transport property along with the proceeding of i-t processes, which is mainly based on the following considerations.**

(1) Electron transport in nanoparticulate films is quite slow, usually in the range of *ms* to *s* depending on electron density in conduction band.[11,12] While, the PSCA technique can record the current transient with a time resolution of *μs* (Electrochemical workstation CHI 660E).

(2) Each group of the combined measurements is done with the same PEC system, that is, the whole three-electrode system is not changed during each series of the combined measurements. Thus, the influence of the film structure, electrolyte diffusion and other PEC cell-related factors can be neglected.

(3) As has been revealed, the band edge are fixed and the chemical capacitance is kept unchanged during the i-t processes (Fig.s8 and Fig.s9).

(4) Electron interface transfer process is much faster than electron transport in TiO_2, in orther words, the latter controls the current transient.[13]

(5) Based on (1) ~ (4), it can be concluded that a larger initial current value and faster decay of the transient corresponds to a faster electron transport (see Fig.s13 for example).

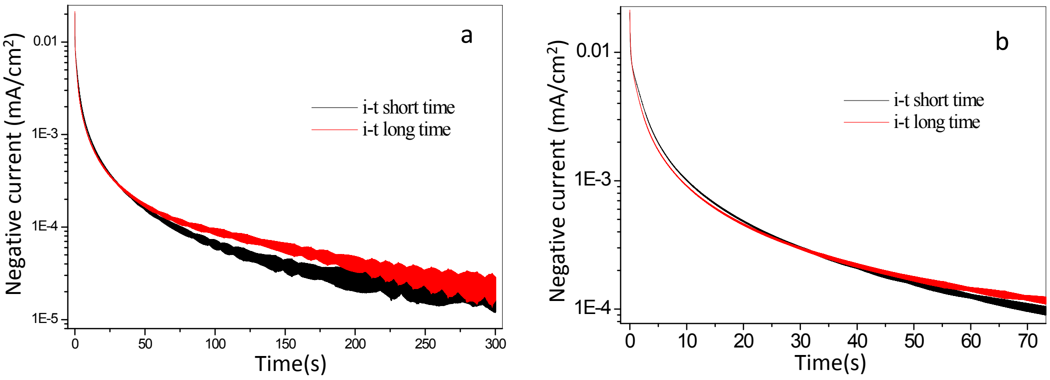

Figure s13 (a) Negative current transient curves measured immediately after a TiO_2 film subjecting to different times of i-t process, (b) an enlarged part in (a). Both (a) and (b) are given in Semi-logarithmic plots to show the faster decay of the transient curve with larger initial current value.

During the first 200 milliseconds all of the transient curves (except for the curve 0s) are coincident and decay steeply (Fig.s12a and c). We tentatively attribute this process to electron injecting into conduction band states. The fast transport of free electrons makes these states becoming populated quickly. The band edge pinning (Fig.s8 and Fig.s9) yields to the same electron injection dynamics no matter how long the i-t processes are preceded.

The decays of these current transient curves after the first 200 ms become slower, which can be attributed to electron diffusing through multiple trapping-detrapping events. The decays of the transient curves of both the D-TiO_2 and R-TiO_2 films show the same trend, that is, a much longer i-t process always gives a lower current value and slower decay (Fig.s12b and d, Fig.s13). Therefore, the combined i-t and PSCA measurements reveal that prolonging the PEC process will continuously deteriorate electron transport property.

S4. Combined measurements of i-t under UV exposure and EIS in dark

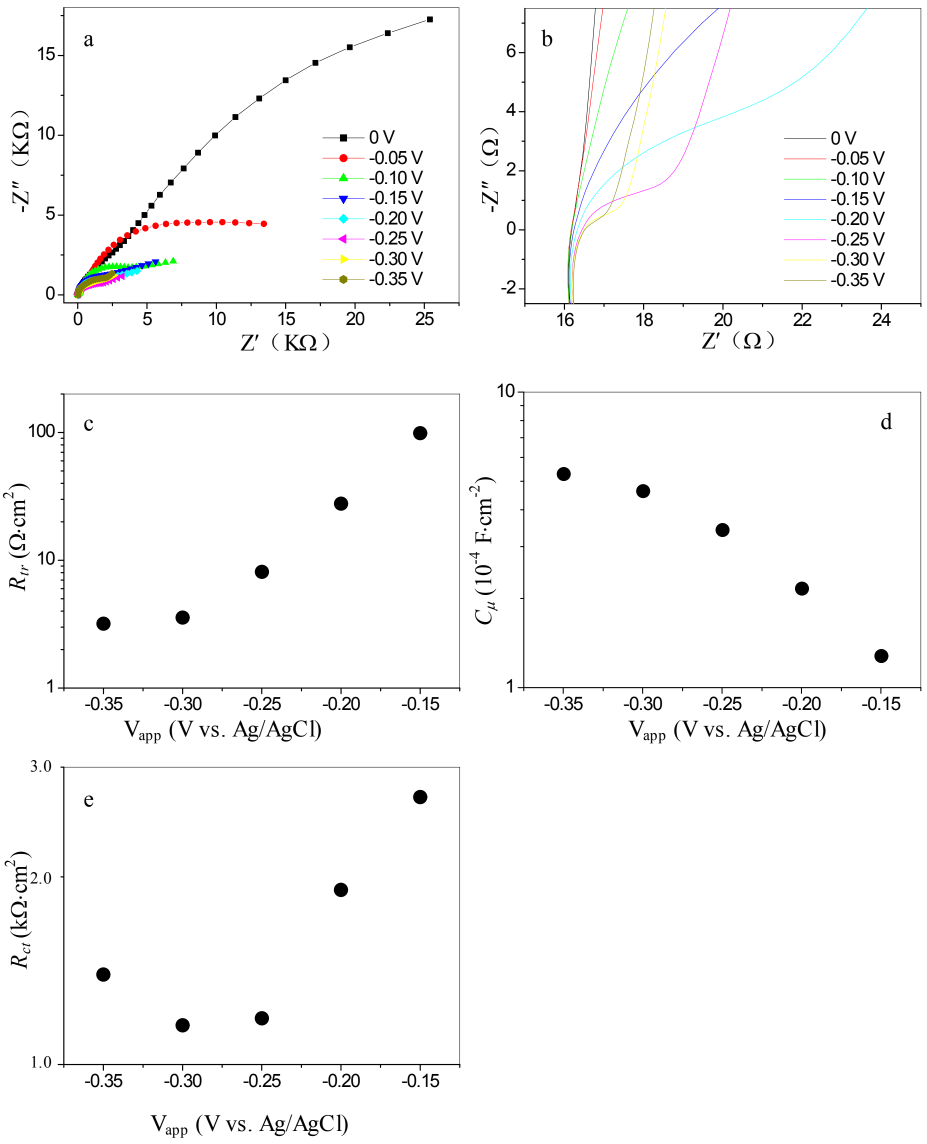

Figure s14. (a) The Nyquist plots of EIS measured in dark immediately when the i-t process under UV light exposure is finished, (b) the enlarged part in high frequency domain of (a), (c~e) the V$_{app}$ dependence of R_{tr}, C_μ and R_{ct} derived by fitting these EIS plots.

Impedance spectra measurements are widely used to acquire information about the dynamics of carriers in PEC systems.[14-16] A series of combined measurements of i-t processes under UV light irradiation and EIS in dark which are controlled by macro command program are carried out. The direct bias (Vapp) dependent evolution of the Nyquist plots is shown in Fig.s14a. When the Vapp is more negative than -0.15V, the EIS give Nyquist plots characteristic of the well known transmission line equivalent circuit mode, that is, a 45° linear part in high frequency domain connecting with an arc at intermediate frequency domain.[14-16] Moreover, the 45° linear part in high frequency domain becomes shortened when more negative Vapp is applied (Fig.s14b). If without subjecting to the i-t process beforehand the Nyquist plots matching the transmission line mode cannot appear only if the Vapp is more negative than -0.60V. The remarkable positive shift of the Vapp is resulted from the i-t process induced positive shift of the energy band edge which has been revealed by the combined i-t/CV and i-t/M-S measurements (Fig.s8 and s9).

The chemical capacitance (C_{μ}), interface charge transfer resistance (R_{ct}) and electron transport resistance (R_{tr}) are obtained by fitting these plots, and the V_{app} dependence of these parameters are given in Fig.s14c~e.

It should be pointed out that another linear part at low frequency domain appears in the Nyquist plots when the Vapp is more negative than -0.1V (Fig.s14a). It can be attributed to the response of charge carrier diffusion in electrolyte. For most cases, electrolyte diffusion is not visible particularly in the dark. While, the significant difference of the EIS measurement herein from common cases lies in that it is carried out immediately following the i-t process. It can be seen from Fig.s8 that the i-t process not only moves the energy band edge positively but also remarkably raises the negative current especially when the bias is more negative than -0.1V. Under this situation, electrolyte diffusion may contribute to the impedance of the system.

References

(1) M. L. Wang, T. He, Y. F. Pan, W. P. Liao, Z. H. Suo and W. Du, *Mater. Chem. Phys.*, 2011, **130**, 1294-1299.

(2) B. Liu and E. S. Aydil, *J. Am. Chem. Soc.*, 2009, **131**, 3985–3990.

(3) A. J. Bard, A. B. Bocarsly, F. F. Fan, E. G. Walton and M. S. Wrighton, *J. Am. Chem. Soc.*, 1980, **102**, 3671-3677.

(4) J. E. Thorne, S. Li, C. Du, G. Qin and D. Wang, *J. Phys. Chem. Lett.*, 2015, **6**, 4083-4088.

(5) R. van de Krol and M. Grätzel, *Photoelectrochemical hydrogen production*, Springer, New York Dordrecht Heidelberg London, 1ed, 2012.

(6) F. Fabregat-Santiago, I. Mora-Seró, G. Garcia-Belmonte and J. Bisquert, *J. Phys. Chem. B*, 2003, **107**, 758-768.

(7) G. Boschloo and D. Fitzmaurice, *J. Phys. Chem. B*, 1999, **103**, 2228-2231.

(8) J. Bisquert, F. Fabregat-Santiago, I. Mora-Seró, G. Garcia-Belmonte, E. M. Barea and E. Palomares, *Inorg. Chim. Acta.,* 2008, **361**, 684-698.

(9) F. Fabregat-Santiago, G. Garcia-Belmonte, J. Bisquert, P. Bogdanoff and A. Zaban, *J. Electrochem. Soc.*, 2003, **150**, E293-E298.

(10) J. Bisquert, *Phys. Chem. Chem. Phys.*, 2003, **5**, 5360-5364.

(11) J. Villanueva-Cab, S.-R. Jang, A. F. Halverson, K. Zhu and A. J. Frank, *Nano Lett.*, 2014, **14**, 2305-2309.

(12) P. E. de Jongh and D. Vanmaekelbergh, *Phys. Rev. Lett.*, 1996, **77**, 3427-3430.

(13) M. Grätzel and A. J. Frank, *J. Phys. Chem.*, 1982, **86**, 2964-2967.

(14) S. Gimenez, H. K. Dunn, P. Rodenas, F. Fabregat-Santiago, S. G. Miralles, E. M. Barea, R. Trevisan, A. Guerrero and J. Bisquert, *J. Electroanal. Chem.*, 2012, **668**, 119-125.

(15) J. Bisquert, *J. Phys. Chem. B*, 2002, **106**, 325–333.

(16) J. Bisquert, G. Garcia-Belmonte, F. Fabregat-Santiago, N. S. Ferriols, P. Bogdanoff and E. C. Pereira, *J. Phys. Chem. B*, 2000, **104**, 2287-2298.